



Facile fabrication of ternary CuO/CuS/ZnS for photodegradation of methylene blue

Muhammad Abudllah¹ · Maryam Al Huwayz² · Norah Alwadai² · Sumaira Manzoor³ · Mehar Un Nisa³ · Peter John¹ · Muhammad Ishfaq Ghor⁴ · Salma Aman⁵ · M. S. Al-Buriah⁶ · Muhammad Naeem Ashiq³

Received: 25 July 2022 / Revised: 10 November 2022 / Accepted: 18 January 2023 / Published online: 9 March 2023
© The Korean Ceramic Society 2023

Abstract

Synthetic dyes play a vital role in our daily life because they are utilized in products ranging from clothing to leather accessories. Unfortunately, these carcinogenic dyes are discharged into water streams any prior process considering the health problems in aquatic life and human beings. It is mandatory to separate noxious materials from wastewater. Semiconductors are viewed as a viable possibility for photocatalytic mineralization of noxious dyes. Herein, facile in situ hydrothermal approach (HT) was utilized for the fabrication of CuO, CuS ZnS, and their ternary CuO/CuS/ZnS nanocomposite. The fabricated CuO/CuS/ZnS nanocomposites were analysed through powder X-ray diffraction (PXRD), Fourier-transform infrared spectroscopy (FTIR), scanning electron microscope equipped with energy-dispersive X-ray (SEM–EDX), and ultraviolet–visible spectroscopy (UV–Vis). Moreover, the optical investigation manifested the bandgap energy value of copper oxide, copper sulphides, zinc sulphides, and ternary CuO/CuS/ZnS nanocomposite, corresponding to 2.63, 3.1, 4.51, and 2.2 eV, respectively, which was estimated from absorption spectrum. Subsequently, the photocatalytic results of CuO, CuS, ZnS, and ternary CuO/CuS/ZnS nanocomposite against methylene blue (MB) dye were 71%, 42%, 45%, and 96%, respectively. The photocatalytic scheme showed the role of hydroxyl radicals and electrons in the photodegradation reaction. Our finding suggests that the fabricated nanocomposite shows superior photocatalytic efficiency towards mineralization of methylene blue which can be used for commercial applications.

Keywords Visible light · Photocatalyst · Methylene blue · Nanocomposite · Photodegradation

1 Introduction

Accelerating global urbanization and industrialization have caused severe environmental and energy problems, threatening all living organisms [1]. Several industrial processes involving textile, ink, paint, and dyeing excessively use toxic organic dyes, with the effluent consisting of large concentrations being discharged into water bodies without any proper treatment, polluting potable water and affecting the aquatic as well as terrestrial living organisms [2]. Among the different kinds of azo dyes, methylene blue (MB) dye is frequently employed for the dyeing process. Although this dye has many benefits to society, it also has many adverse effects on living organisms such as mild bladder irritation, dizziness, headache, increased sweating in joints, neural disorder, etc. [3, 4].

Therefore, to solve the above addressed issues, there is an urgent need to use advanced technology to purify wastewater from toxic dyes [5]. Nowadays, several techniques such as

✉ Muhammad Naeem Ashiq
naeembzu@bzu.edu.pk

- ¹ Department of Chemistry, Government College University Lahore, Katchery Road, Anarkali, Lahore 54000, Punjab, Pakistan
- ² Department of Physics, College of Science, Princess Nourah bint Abdulrahman University, P.O. Box 84428, Riyadh 11671, Saudi Arabia
- ³ Institute of Chemical Sciences, Bahauddin Zakariya University, Multan 60800, Pakistan
- ⁴ Department of Chemistry, Government Murray College, Sialkot 51141, Pakistan
- ⁵ Institute of Physics, Khwaja Fareed University of Engineering and Information Technology, Abu Dhabi Road, Rahim Yar Khan 64200, Pakistan
- ⁶ Department of Physics, Sakarya University, Sakarya, Turkey

membrane separation [5, 6], ozone oxidation [7], adsorption [8, 9], sedimentation [10], Fenton oxidation [11], and photocatalytic degradation [12, 13] have been employed for the treatment of chemical effluents [14]. However, the above-mentioned techniques have various drawbacks. Membrane separation, adsorption, and oxidation are non-economical, cannot degrade toxic dyes completely, and produce multiple secondary by-products [15]. On the other hand, the sedimentation process reduces the suspended particles from the wastewater, but cannot remove pathogen and dissolved toxic substances [16]. However, owing to low energy consumption, reduced secondary pollutants, low cost, simple operation and great efficiency, the photocatalysis method has garnered significantly more attention than others [17, 18].

In the last few decades, semiconductor based nanostructured catalysts can effectively degrade several organic compounds attributed high stability, large surface area, and large surface activity [19, 20]. In particular, metals and semiconductors nanomaterials are considered potential candidates to degrade harmful dyes. Metals such as palladium, gold, and silver nanoparticles are also good materials for the degradation of dyes within several hours. Despite the exhibition of superior photocatalytic efficiency, these metals are costly [21]. Because of their large bandgaps, benchmark semiconductor photocatalysts such as zinc oxide and titanium dioxide can only captivate 5% of ultra violet light for photocatalysis, restricting their use as an environmental purifier under the source of sunlight [22, 23]. The task therefore is to create a photocatalyst with a small bandgap to make efficient use of visible light. However, researchers are focused on developing semiconductor-based photocatalysts that exhibit superior photocatalytic efficiency, stability, and economy than precious metals [14, 24, 25]. Several researchers studied nanophotocatalysts to elaborate the efficiency of semiconductor materials such as CuO [26], ZnO [27], CuS [28], NiO [29], SnO₂ [30] and ZnS [31]. Abi M. Taddesse et al. described fabrication of zinc oxide based Cu₂O/ZnO/Ag₃PO₄ nanosized composite for mineralization of MO with 78% efficiency [32]. Sara Behjati et al. studied the

Cu₂O–CuO nanocomposite employed for MB 55% degradation under visible light illumination [33]. Moreover, several methods are available to delay the electron (e⁻)-hole (h⁺) recombination process such as composite, doping, and engineering in the material surface. The visible light energy used to produce electron–hole pairs is economical and environmentally friendly; thus, synthesized nanophotocatalysts favour green chemistry. So in the present work, the low bandgap material was selected so that it can absorb visible light and their composite to stop the e⁻/h⁺ pair recombination that will enhance the efficiency of the materials for the degradation of MB.

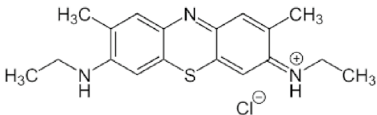
This work reports the fabrication of ternary CuO/CuS/ZnS nanocomposite to improve nanomaterial photocatalytic properties via the facile one-pot hydrothermal method. The synthesized nanostructure was analysed by PXRD, FTIR, SEM, EDX, and UV–Vis spectroscopy. The BET technique was utilized to examine the surface area of the fabricated nanostructure. Moreover, the photocatalytic efficacy of the ternary CuO/CuS/ZnS nanostructure was examined by the mineralization of methylene blue (MB) under visible light. The main aim of this work comprises (1) the fabrication of the novel ternary CuO/CuS/ZnS nanocomposite, (2) the study of physical, chemical, and structural properties, and (3) the determination of the potential capability of nanomaterials towards methylene blue degradation.

2 Experimental part

2.1 Chemicals

Chemical reagents including Cu(NO₃)₂ (> 98%), KOH (> 85%), K₂S (> 95%), ZnCl₂ (> 98%), and ethanol (96%) were used as such without prior purification steps for the fabrication of CuO, CuS, ZnS, and CuO/CuS/ZnS nanomaterials. The commercial methylene blue (MB) azo dye was purchased from Sigma-Aldrich, and its chemical structure and λ_{max} are given in Table 1.

Table 1 The structural expression and λ_{max} of the MB dye

Name of dyes	Structure	λ _{max}
Methylene Blue		665 nm

2.2 Fabrication of CuO nanoparticles

Cu(NO₃)₂ and KOH were used as precursors to synthesize nanosized CuO material and act as the reducing agent, respectively. In the first step, 0.1 M Cu(NO₃)₂ and 2.0 M KOH were poured gently with continuous stirring to make a uniform solution. Furthermore, a solution was transformed into a hydrothermal reactor and kept under an electric furnace for 10 h at 180 °C. Next, the obtained material was rinsed with C₂H₅OH and deionized H₂O, dehydrated in a drying oven, and then annealed at 500 °C for 4 h. At last, the material was annealed for 4 h at 500 °C.

2.3 Fabrication of CuS nanoparticles

The hydrothermal technique has been used for the preparation of the CuS nanomaterial. An equimolar ratio (0.1 M) of an aqueous solution of K₂S and copper nitrate was mixed and subsequently continuously stirred on a magnetic hot plate. Then reaction mixture was poured into a hydrothermal reactor (HR) at 100 °C for 24 h. The as-synthesized material was rinsed with ethanol and H₂O and dehydrated in an electric oven for 14 h at 70 °C. The synthesized material was saved in a vacuum bottle for further material analysis.

2.4 Fabrication of ZnS nanoparticles

In the synthesis of ZnS, 0.1 aqueous solutions of K₂S were prepared and mixed into 0.1 M ZnCl₂ solution. After 5 h of continuous agitating on the magnetic hot plate, pale yellow precipices were obtained. The synthesized precipitate was separated by centrifugation. Finally, the precipitate was dehydrated in electric oven overnight, then ground and saved in air tight vials.

2.5 Preparation of CuO/CuS/ZnS nanocomposite

CuO/CuS/ZnS ternary nanocomposite was also prepared through a hydrothermal route. In this case, equimolar ratio (0.1 M) solution of copper nitrate was mixed with potassium sulphide solution followed by the insertion of 0.5 g calcined copper oxide and 0.5 g of ZnS nanoparticles on the magnetic plate to homogenize the mixture. Further, the reaction solution was transferred into a hydrothermal reactor and heated for 24 h at 200 °C. The obtained materials were washed with centrifugation with C₂H₅OH and DI H₂O, dried, ground, and stored for further characterization.

2.6 Characterizations

The crystallinity, purity, and structure of nanopowders were investigated by XRD using Bruker D2 Phaser with copper K alpha radiation (1.5040 Å) at 4°/min in 2θ range of 20 to 80°.

Moreover, EDX and SEM (Nova Nano SEM-450) analyses of as-synthesized materials were done to measure the purity and quantitative amount of the elemental composition at 77 K. The UV–visible spectrophotometer (Agilent Carry 60) was employed to investigate the optical features of nanomaterials recorded between of 200–800 nm. The FTIR (JASCO 6800) was used to measure the chemical species in the range of 400–4000 cm⁻¹. The textural behaviour of all the fabricated photocatalyst was investigated with Brunauer–Emmett–Teller (BET) analysis using NanoNova 2200e Quantachrome under N₂ adsorption/desorption at 77 K. The EIS analysis was conducted using an electrochemical workstation (PG-STAT 204) with three electrode system under 2.0 M KOH.

2.7 Photocatalytic assessment

The photocatalytic efficacy of the generated materials was calculated by mineralization of MB using visible light (200 W) irradiation at ambient condition (25 °C and pH=6.5). A 1 × 10⁻⁴ M dye solution of methylene blue was made in 200 mL of DI H₂O. 0.1 g of nanomaterials was introduced into an organic dye solution and kept under dark for 30 min for achieving sorption mechanism among the dye and photocatalyst. After that, the mixture aliquot was collected to measure the starting concentration of the dye mixture at wavelength 664 nm. Moreover, the dye solution was irradiated with a visible source, and an aliquot of the solution was drawn from the solution after a regular interval of 20 min. The collected materials were centrifuged to separate the nanocatalyst, and the effect of light in the presence of nanomaterials measured with a UV visible spectrophotometer. The mineralization percentage of dye is measured by the following expression [34]:

$$\% \text{ Degradation efficiency} = \frac{c_0 - c}{c_0} \times 100, \quad (1)$$

where C_0 expresses the initial concentration and C_t represent the dye concentration at any time in the reaction, respectively. Additionally, various scavengers, i.e., PBQ (superoxide radicals ($\bullet\text{O}_2^-$)), EDTA-2Na (holes (h^+)), AgNO₃ (electrons (e^-)), and DMSO (hydroxyl radicals ($\bullet\text{OH}$)) were applied to capture radicals. The repeatability analysis was also measured by employing CuO/CuS/ZnS photocatalyst against methylene blue dye by rinsed used photocatalyst, centrifuge, dried, and recycled for the succeeding cycle.

3 Result and discussion

3.1 Phase analysis

Figure 1(a–d) represents the XRD pattern for CuO, CuS, ZnS, and CuO/CuS/ZnS nanocomposites. The different diffraction

patterns observed at 2θ values 32.43° , 37.89° , 49.96° , 55.64° , and 66.42° correspond to (103), (202), (301), (230), and (026) hkl values and have cubic crystal structure (PDF = 01-078-1588) of CuO nanoarray (Fig. 1(a)). The diffraction peaks located at 36.63° , 38.93° , 48.85° , 56.89° , 65.76° , and 66.86° with (hkl) values (104), (105), (112), (109), (206), and (118) show the hexagonal structure of CuS (PDF = 01-085-0620). The characteristic peaks appearing at 32.01° , 34.42° , 47.62° , 56.70° , 68.01° , and 76.98° , indexed at (220), (201), (200), (311), (400), and (420), suggesting the cubic phase of ZnS, and the presence of all these indexed in the diffraction pattern of CuO/CuS/ZnS depicted the fabrication of the nanocomposite. The average nanoparticle size of CuO, CuS, ZnS, and CuO/CuS/ZnS belonging to 3.86 nm, 13.63 nm, 26.231 nm, and 3.44 nm was measured by Scherrer expression [35].

$$D = \frac{K\lambda}{\beta \cos\theta}, \quad (2)$$

where β is the full width at half maxima, K is the Scherrer constant, and D represents the particle size. The dislocation

density of the fabricated material was investigated by employing Eq. 3 [36].

$$\delta = \frac{1}{D^2}. \quad (3)$$

The dislocation density of copper oxide, copper sulphide, zinc sulphide, and ternary nanocomposite was $0.774133 \text{ m}^2 \times 10^{15}$, $0.003924 \text{ m}^2 \times 10^{15}$, $0.000825 \text{ m}^2 \times 10^{15}$, and $0.086126 \text{ m}^2 \times 10^{15}$, respectively.

Moreover, FTIR technique was used to study chemical structure and purity of nanomaterials as shown in Fig. 2(a–d). The transmittance curve at $3800\text{--}3000 \text{ cm}^{-1}$ are owing to a strong adsorption band of hydroxyl groups on the interfaces of the photocatalyst [37]. The characteristic peaks of copper oxide at 1644.87 cm^{-1} , 1555.64 cm^{-1} , 1385.54 cm^{-1} , and 1099.43 cm^{-1} correspond to nitrogen–oxygen stretching band [38]. CuS spectra exhibited peaks at 713.66 cm^{-1} , 1032.77 cm^{-1} , 1501.51 cm^{-1} , and 1620.56 cm^{-1} with respect to copper sulphide, nitrogen–oxygen stretching vibration, nitrogen–hydrogen bending vibration, and oxygen–hydrogen bending vibration, respectively [39]. ZnS peaks located at 705.94 , 1020 , and 3213.4 cm^{-1} are ascribed to ZnS, S–O, and O–H [40]. CuO/CuS/ZnS peaks located 732.65 cm^{-1} , 1016.48 cm^{-1} , 1521.91 cm^{-1} , and 3720 cm^{-1} correspond to Cu–S, S–O stretching vibration, N–O stretching vibration, and oxygen–hydrogen bending vibration [41, 42], respectively.

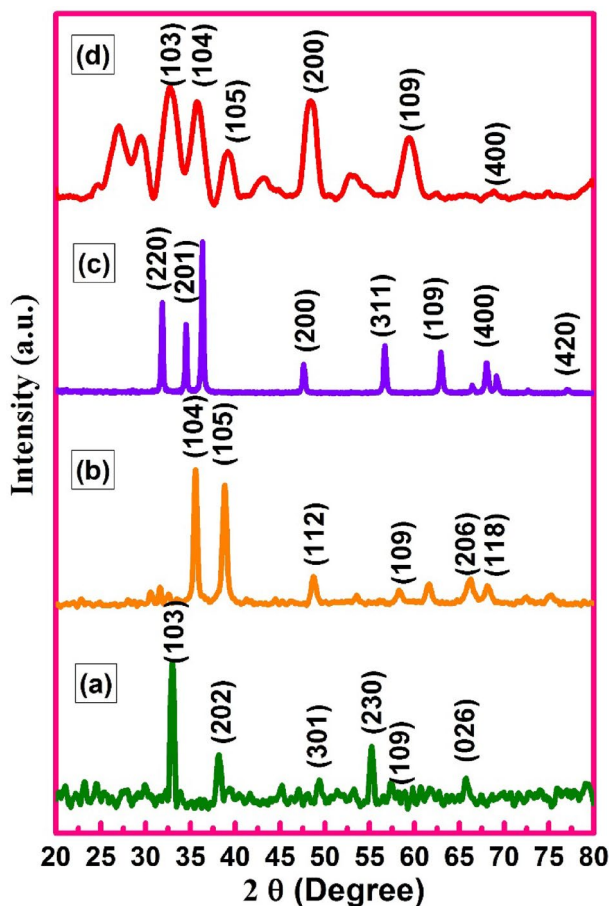


Fig. 1 XRD diffraction patterns for **a** copper oxide, **b** copper sulphides, **c** zinc sulphides, and **d** CuO/CuS/ZnS ternary nanocomposite

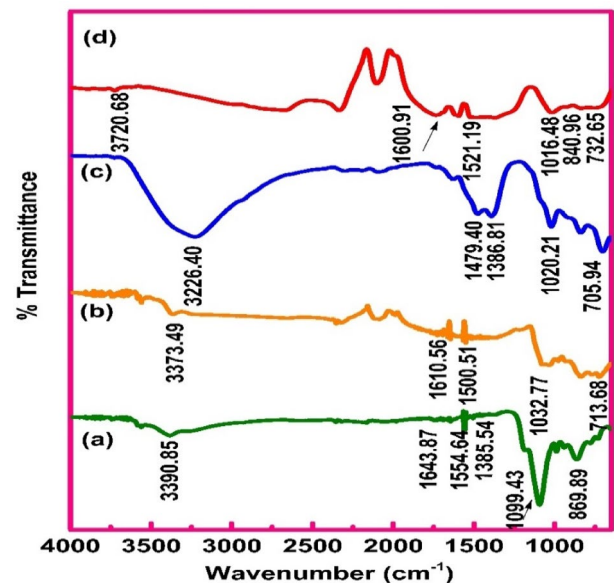


Fig. 2 FTIR spectra for **a** copper oxide, **b** copper sulphides, **c** zinc sulphides, and **d** ternary nanocomposite

3.2 Morphological and textural investigation

Figure 3 illustrates the morphology of the fabricated ternary nanocomposite, analysed with an SEM image. The morphological properties of the CuO/CuS/ZnS ternary composite at 10,000 \times and 50,000 \times are given in Fig. 3(a, b) with spherical, uniformly distributed agglomerates due to the enormous surface energy of the material during preparation. The large interfaces provide a significantly large number of active zone for photocatalysis. The surface plot, plot profile, and particle size 39.84 nm of the synthesized nanocomposite were calculated by ImageJ software as depicted in Fig. S1.

Subsequently, EDX confirms the existence of different elements present in the nanostructure, as display in Fig. 3(c–d). The EDX result indicates that the synthesized nanocomposite contains elements O, S, Cu, Zn as well as Au. Besides, the existence of Au peak was not taken into account due to sample-supported species.

Figure 4(a, b) illustrates the BET analysis to calculate the interface area and distribution of pore size in the ternary CuO/CuS/ZnS nanocomposite. The fabricated CuO/CuS/ZnS nanocomposite has increased reactive sites due to the larger interface area (45.37 m²/g) with pore size 0.021 m²/g, resulting in enhancing the photocatalytic efficiency of the nanophotocatalysts.

3.3 Optical analysis

The optical analysis of nanocomposite was obtained using a UV–visible spectrophotometer at $\lambda = 200\text{--}800$ nm at ambient temperature, as shown in Fig. 5(a–d). An optical absorption spectrum was also employed to investigate the bandgap value using Tauc's profile technique with allowed transition conveyed by Mott and Davis theory through Eq. 4 [43, 44]:

$$\alpha h\nu = A(h\nu - E_g)n/2. \quad (4)$$

Here, α are absorption coefficient, h represents Planks constant, ν display the light frequency, c are speed of light, E_g are optical bandgap and A for absorption. The measured bandgap value of CuO, CuS, ZnS, and CuO/CuS/ZnS corresponds to 2.63 eV, 3.1 eV, 4.51 eV, and 2.2 eV; respectively. It was measured at the point where the straight line intersects the x -axis as shown in Fig. 6 [45]. The lower the bandgap energy of the composite, the greater is the movement of electrons to the C.B (conduction band) in the existence of visible source [46]. Several parameters directly affect the bandgap value, such as defects, crystallite size, and specific area.

3.4 Electrochemical analysis

The EIS investigation was employed to study the charge transfer and recombination behaviour of the synthesized material with three electrodes configuration and the

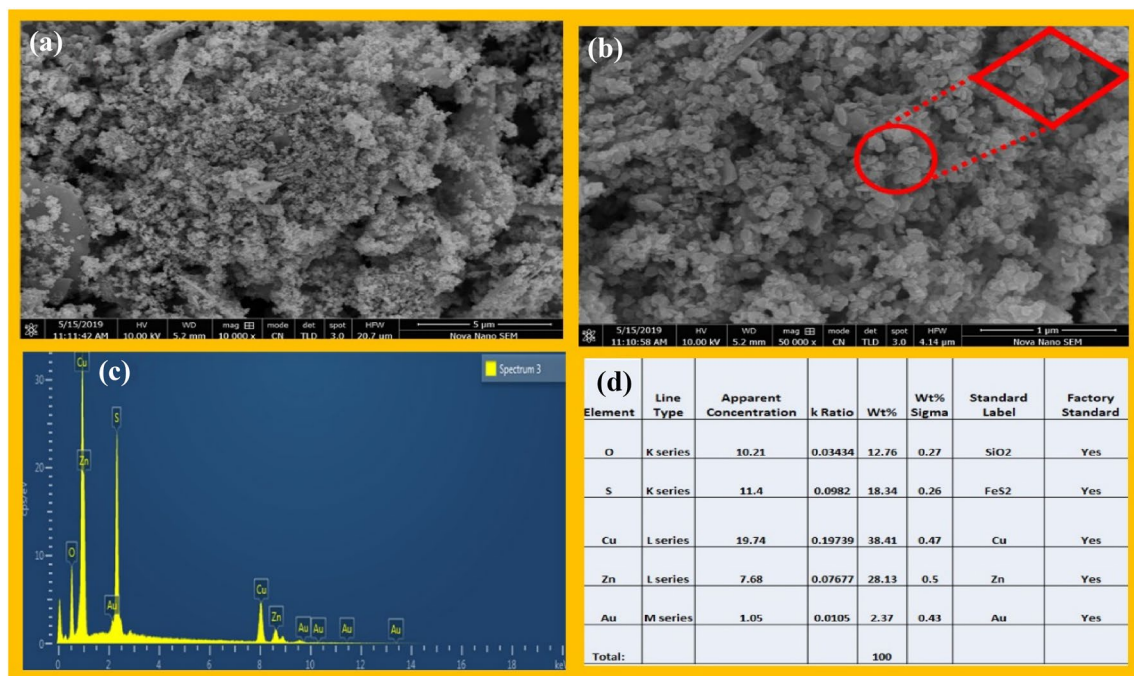


Fig. 3 a, b SEM micrograph of ternary nanocomposite at low (5 μm) and high magnification (1 μm), c EDX spectrum, and d EDX of atomic % able CuO/CuS/ZnS

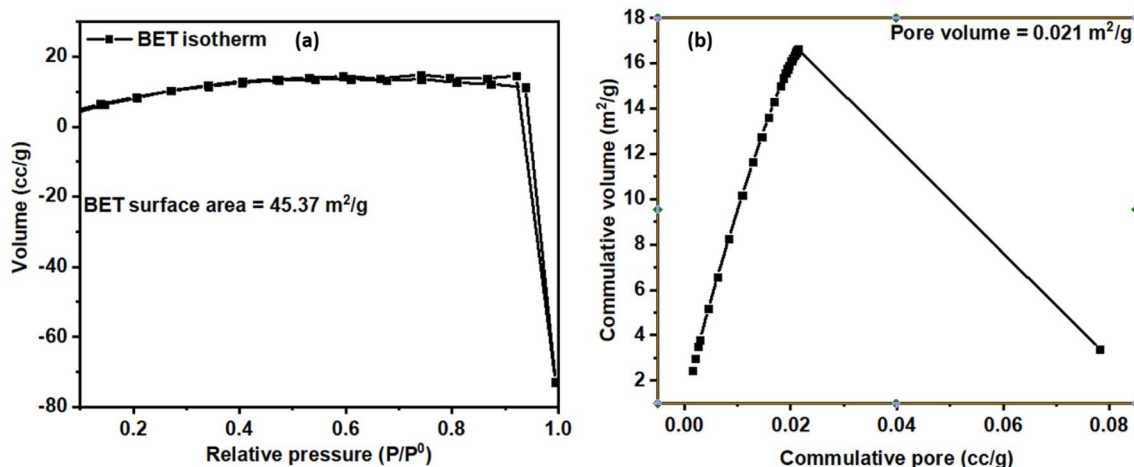


Fig. 4 a BET isotherm and b pore volume of CuO/CuS/ZnS nanocomposite

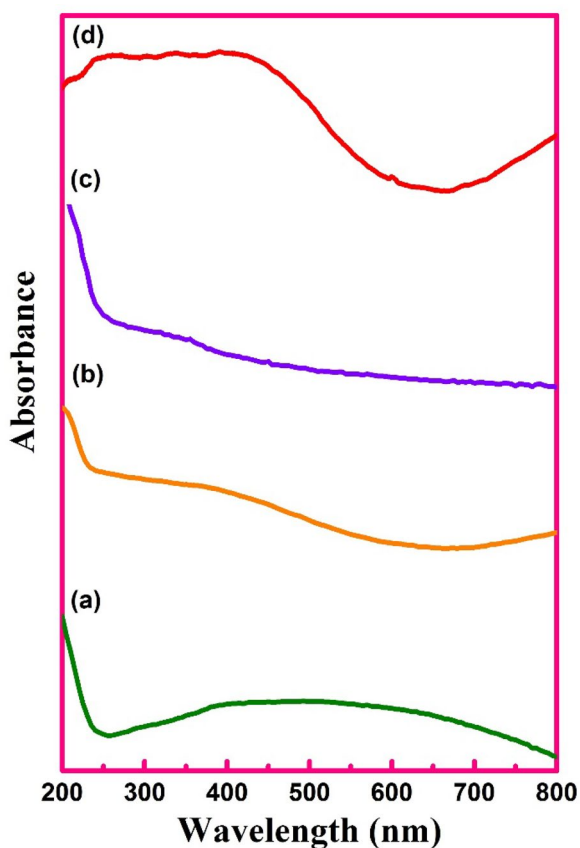


Fig. 5 UV-visible spectra for a copper oxide, b copper sulphide, c zinc sulphide, and d ternary CuO/CuS/ZnS nanocomposite

fabricated material acts as a working electrode as shown in Figs. 6(a), 7 Constant phase element (CPE) and charge transfer resistance (Rct) at the photocatalyst/electrolyte interface are responsible for the semicircle seen in the EIS spectra. The curved line that results from the Warburg

impedance (ZW) depicts the ion diffusion route in the basic solution. The obtained Rct for CuO, CuS, ZnS, and CuO/CuS/ZnS are 0.7, 2.8, 4.1 and 6.1 Ω , respectively. Among these, reduced resistance value by the development of the ternary nanocomposite, furthermore supporting these, enhances the charge migration and isolation of photoinduced carriers. In conclusion, EIS analysis verifies that the CuO/CuS/ZnS photocatalyst is superior, since the addition of CuO to ZnS improves the efficiency with which photogenerated e/h⁺ pairs are separated and transferred.

3.5 Photocatalytic degradation

The mineralization of MB dye with synthesized copper oxide, copper sulphide, zinc sulphide, and ternary nanocomposite of CuO/CuS/ZnS nanocomposite as photocatalyst under the source of visible light irradiation is illustrated in Fig. 8(a). The degradation of methylene blue was measured at 664 nm. After adding 0.1 g photocatalyst in the 100 ml dye solution, the absorption value starts decreasing, indicating the degradation of the dye solution. It was noted that 71%, 42%, 45%, and 96% of dye degraded after 160 min, with CuO, CuS, ZnS, and CuO/CuS/ZnS as nanophotocatalyst, respectively. The kinetics for the dye degradation rate was followed by pseudo-first-order kinetics estimated with given formula 5 [47]:

$$\ln \frac{C_t}{C_o} = kt. \quad (5)$$

Here, C_t represents the concentration at any time, C_o represents the starting dye quantity and k is mineralization rate constant. The degradation rate constant was determined to be 0.007, 0.00323, 0.00328, and 0.018 for CuO, CuS,

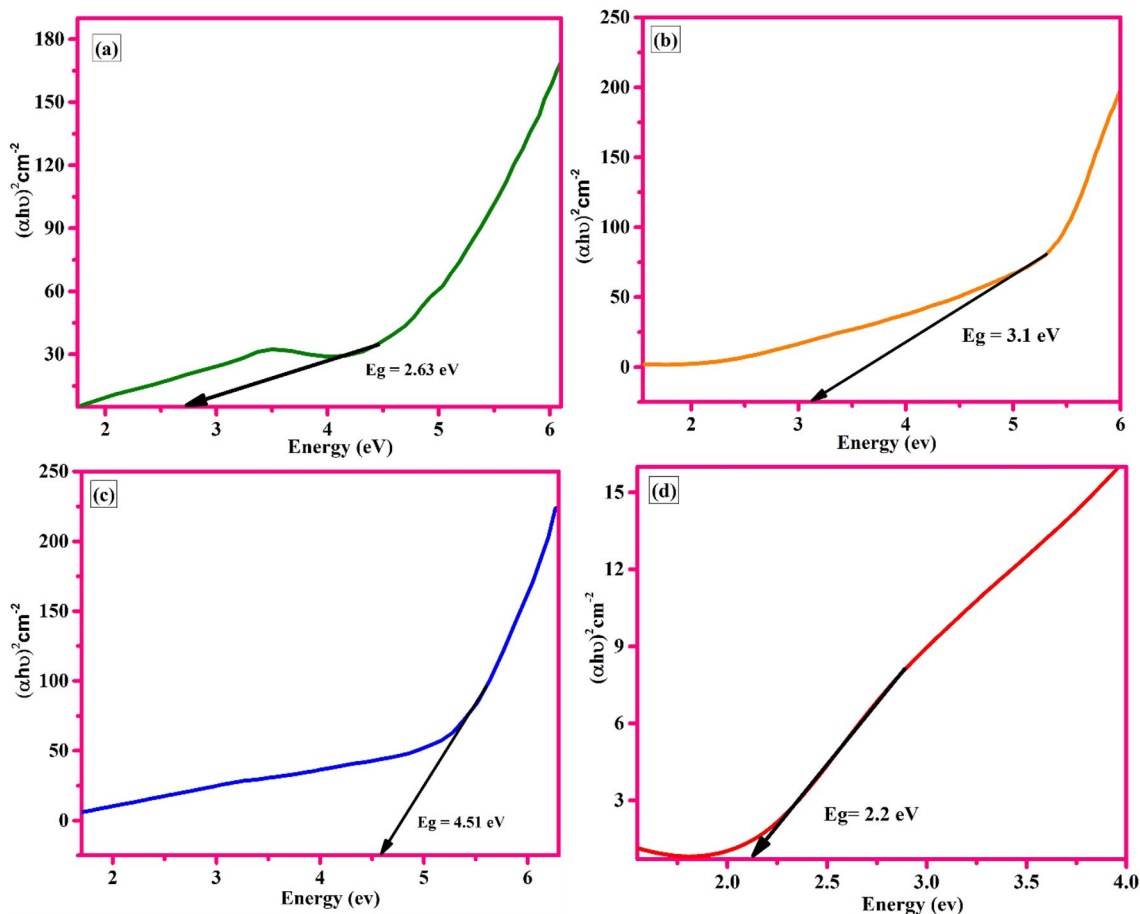


Fig. 6 Tauc plots for a CuO, b CuS, c ZnS, and d CuO/CuS/ZnS

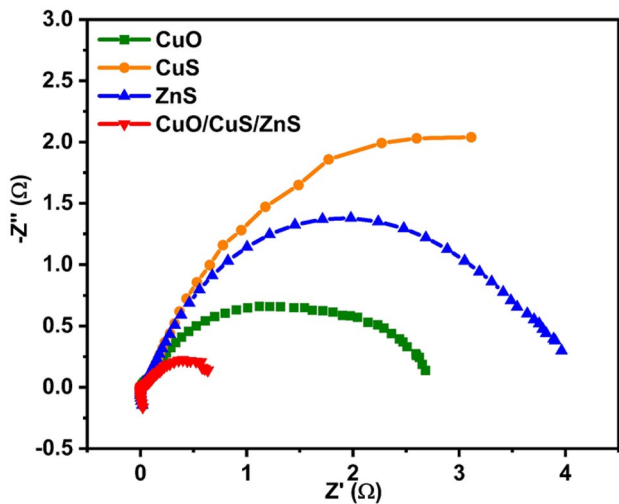


Fig. 7 Nyquist polarization plot of all fabricated materials

ZnS, and CuO/CuS/ZnS, respectively. A comparative study among CuO, CuS, ZnS, and CuO/CuS/ZnS is shown in Tables 2 and 3.

3.5.1 Photocatalytic mechanism

The photodegradation mechanism, explained based on effective charge separation and band positions, can be calculated by the empirical formula [48]:

$$E_{VB} = X - E_H + 0.5E_g, \tag{6}$$

$$E_{CB} = E_{VB} - E_g. \tag{7}$$

Here, E_{VB} represents the potential of valence band, X shows the semiconductor electronegativity, E_{CB} represents the potential of conduction band, and E_H the energy processed by an electron at a hydrogen scale (4.5 eV) [49]. The value of X for CuO, CuS, and ZnS are 5.8 eV, 5.27 eV, and 5.06 eV, respectively [50, 51]. The calculated conduction band potentials were -0.015 , -0.78 , -1.695 eV, and the valence band potentials were 2.615 , 2.32 , and 2.815 eV for CuO, CuS, and ZnS, respectively. The band's potentials were calculated using optical energy bandgap (E_g) 2.63, 3.1, 4.51 eV for CuO, CuS, and ZnS, respectively, calculated from UV results. A scheme was proposed based on the

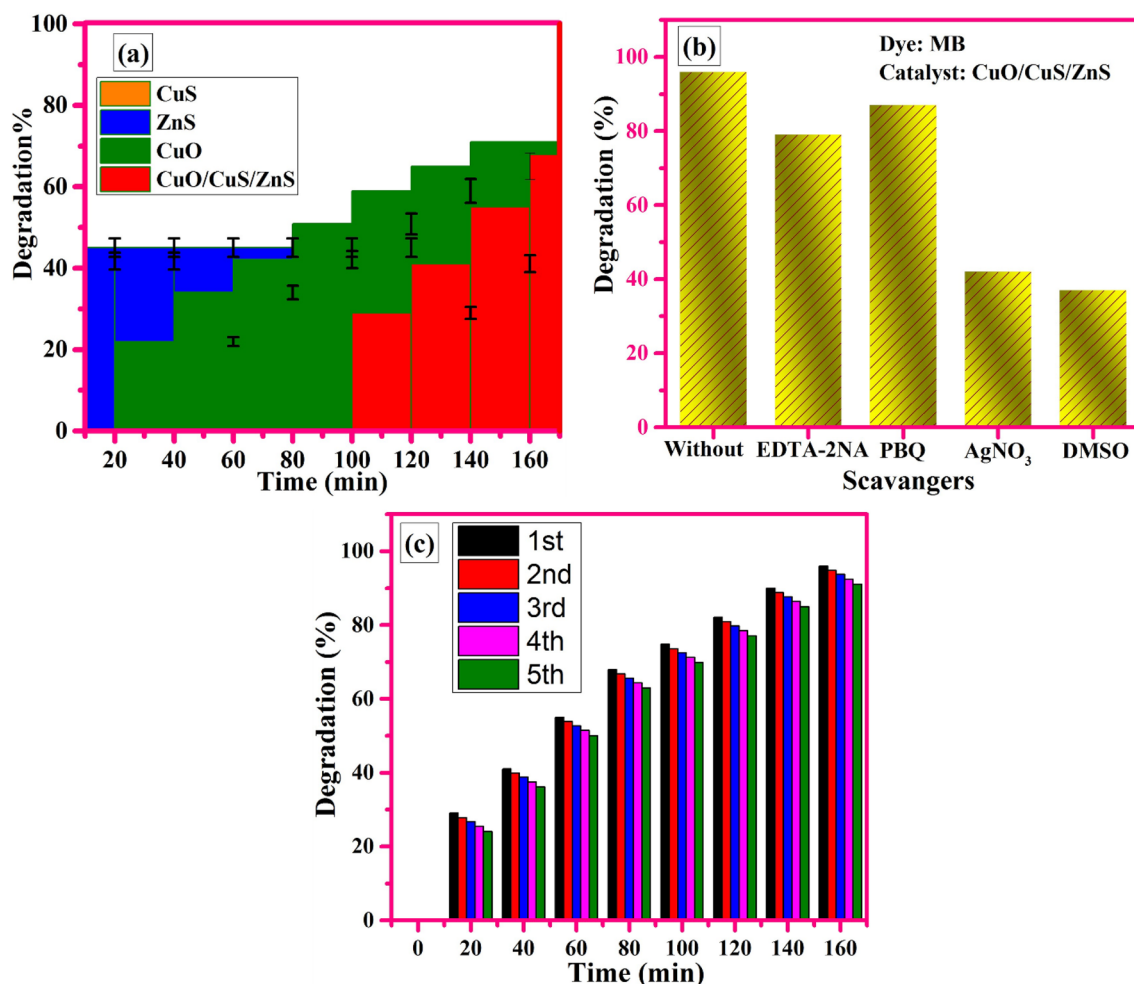


Fig. 8 a Percent degradation of all synthesized materials, b degradation efficacy (%) by adding different scavengers, and c recyclability profile

Table 2 Percentage degradation under visible and specific rate constant for the prepared materials

Sr. No.	Materials	% Degradation	Time (min)	Rate constant
1	CuO	71	140	0.00711
2	CuS	42	100	0.00323
3	ZnS	45	120	0.03280
4	CuO/CuS/ZnS	96	160	0.01811

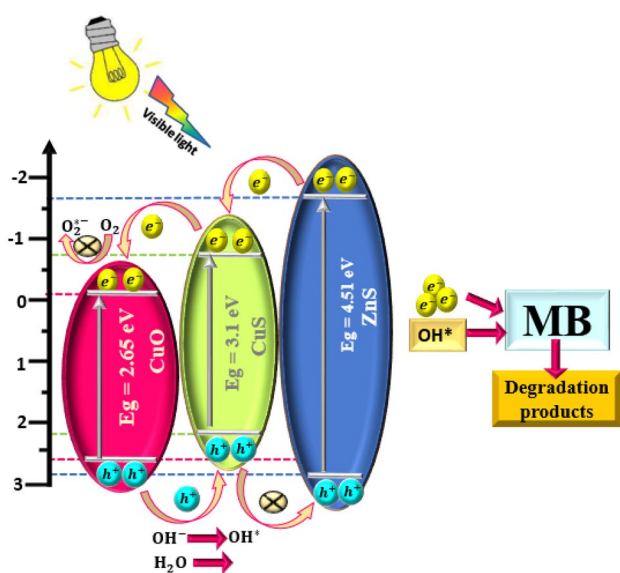
band's potential, namely Scheme 1, to illustrate the charge separation, migration, and photodegradation of MB molecules (Scheme 1).

The mineralization of methylene blue was initiated by the nanomaterials by the photoexcitation process at the surface. When nanomaterials were irradiated with the source of visible light, it resulted in the generation of e^-h^+ pair by excitation of e^- to the C.B of copper oxide, copper sulphide, and zinc sulphide from the valence band (VB), leaving holes in

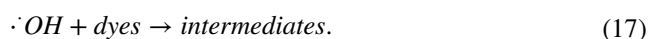
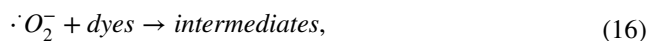
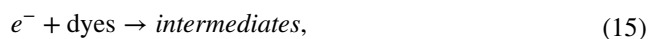
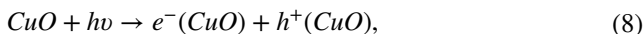
the valance band. From the above calculation, the CB of CuS is smaller than that of ZnS, so electrons move from the CB of ZnS to copper sulphide. Also the CB of CuO is smaller than that of CuS, so the electron further moves from the CB of CuS to the conduction band of CuO. Upon reaching CuO CB, unfortunately, CuO's CB potential is -0.015 eV, which is lower than the potential required to convert O_2 into $\cdot O_2^-$, -0.33 eV [52]. So, the electrons directly react with the dye molecules. Alternatively, the holes transport from the VB of CuO to the valence band of CuS for charge conservation, but not from the valence band of CuS to the valence band of ZnS because of being less favourable. The holes at the VB of copper sulphide and zinc sulphide are fruitful due to the undesirable potential capacity (2.32 eV) for oxidation and reduction reaction ($\cdot OH/OH^-$ 1.99 eV and $\cdot OH/H_2O$ 2.27 eV) [53]. The holes at the VB of CuS and ZnS interact with OH^- and H_2O and generate $\cdot OH$. So, using such a scheme, the process is described systemically, as principal reactive species are electrons and hydroxyl radicals produced. The decomposition of MB dyes occurs via an interaction with hydroxyl

Table 3 Comparative study among synthesized nanomaterials and reported nanomaterials

Sr. no.	Catalysts	Dye	Light	% Degradation	Ref.
1	Ag-decorated ZnO	4-NP	Natural UV-filtered sunlight	85	[54]
2	ZnS	MO	Visible light	12	[55]
3	CuS	Methylene blue	UV light	43	[56]
4	CdS NRs	Methylene blue	UV light	34	[57]
5	ChPA/ZnS	Cresol red	Sunlight	75	[58]
6	Al ₂ O ₃ -doped Mn ₃ O ₄	Brilliant cresol blue	Visible light	50–65	[59]
7	S-doped ZnO	Methylene blue	Visible light	85.8	[60]
8	V-doped Mn ₃ O ₄ NP	Methylene blue	Visible light	82.5	[61]
9	Al-doped Mn ₃ O ₄	Malachite green	UV light	90	[62]
10	Mn ₃ O ₄	Acridine orange	UV–visible	47.3	[63]
11	CuO/CuS/ZnS	Methylene blue	Visible light	96	Present

**Scheme 1** Representation of the photodegradation mechanism

group and electrons producing intermediates. By introducing $\cdot\text{OH}$ (DMSO) and e^- (AgNO_3)-type scavengers instead of hydroxyl and hole-type scavengers, the radical capture experiment validates the function of hydroxyl radicals and electrons in the mineralization mechanism. (Fig. 8(b)). The oxidation and reduction process of oxygen-containing species, including hydroxyl radical (OH^-) in water, is shown as a schematic diagram in Scheme 1. Therefore, the mineralization of methylene blue dye can be attributed to these reactive species produced by the nanomaterials which react with the dye. The CuO/CuS/ZnS photocatalyst mechanism with reactions is explained as follows:



Additionally, an experiment on the recyclability of the generated catalyst was carried out, showing that it is effective for up to five cycles (Fig. 8(c)). Hence, several factors, including dispersion of catalyst, size, and specific surface area, can limit or enhance the photocatalytic process because organic dye's photodegradation occurs on the interfaces of nanomaterials. The results obtained from the present investigation was compared with a previous work and are given in Table S1. The outcome showed that visible light-active CuO/ZnS/CuS composite showed much better results and can be considered as good candidate for degradation pollutants.

Analytik Jena's multi N/C UV HS TOC analyser was used to look at the photodegradation of MB. The absolute value of TOC decreased from 96.2 to 12.16 mg L^{-1} as confirmed from Fig. 8 with an efficiency of nearly 87.36%

(Fig. 9 inset). The photocatalytic efficacy (Fig. 8) shows almost 96% mineralization over CuO/CuS/ZnS, and the leftover total organic content may be related to the presence of intermediates before they are completely mineralized into carbon dioxide (CO₂) and water.

4 Conclusion

A ternary nanocomposite based on CuO, CuS, and ZnS was fabricated through facile hydrothermal methods. The characterized results of microscopy and spectroscopy revealed the crystalline nature, purity, and structure of nanomaterials, presence of active substances, indicated uniform aggregation and crystallite size (39 nm), and showed the elemental composition of ternary nanocomposite and bandgap (CuO, CuS, ZnS, and CuO/CuS/ZnS are 2.63 eV, 3.1 eV, 4.51 eV, and 2.2 eV, respectively) from the absorption spectra of nanomaterials, respectively. The BET investigation was employed to study the interfacial area of CuO/CuS/ZnS which was 45.37 m³g⁻¹. The photocatalytic efficiency of the synthesized copper oxide, copper sulphide, zinc sulphide, and ternary nanophotocatalyst was tested to degrade MB under visible source of light irradiation. Moreover, CuO, CuS, and ZnS exhibited photocatalytic efficiency of 71%, 45%, and 42%, respectively, and photocatalytic measurement of ternary-based nanocatalyst exhibited 96% degradation rate within 160 min. The EIS analysis shows the R_{ct} value for CuO, CuS, ZnS, and CuO/CuS/ZnS are 0.7, 2.8, 4.1 and 6.1 Ω, respectively. The superior photocatalytic result of ternary nanosized composite was attributed to the small bandgap, small crystallite size, and large surface area. Thus, the CuO/CuS/ZnS nanocomposite is a novel kind of promising photocatalyst that can be explored for environmental purification

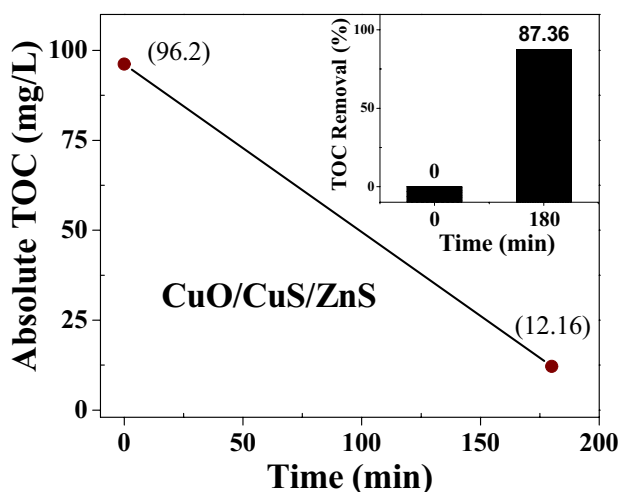


Fig. 9 Absolute TOC values for CuO/CuS/ZnS-dispersed MB solution irradiated for different times with removal efficiency in the inset

and industrial effluent treatment in the future, particularly in dyeing industries.

Supplementary Information The online version contains supplementary material available at <https://doi.org/10.1007/s43207-023-00287-4>.

Acknowledgements The authors express their gratitude to Princess Nourah bint Abdulrahman University Researchers Supporting Project number (PNURSP2023R439), Princess Nourah bint Abdulrahman University, Riyadh, Saudi Arabia. M. N. Ashiq is highly thankful to Bahauddin Zakariya University, Multan, for financial support.

Data availability Since no data sets were created during the time period covered by this paper, data exchange is not relevant.

Declarations

Conflict of interest No potential conflict of interest was reported by the author.

References

- D. Xu, L. Chen, X. Zhang, L. Li, Q. Ding, G. Zhu, Preparation of Co₃O₄/niobate composite photocatalysts by ZIF-67 derivative for photocatalytic property of water splitting. *Surfaces and interfaces* **27**, 101514 (2021)
- V. Gupta, S. Khamparia, I. Tyagi, D. Jaspal, A. Malviya, Decolorization of mixture of dyes: A critical review. *Global Journal of Environmental Science Management* **1**, 71–94 (2015)
- L. Vutskits, A. Briner, P. Klauser, E. Gascon, A.G. Dayer, J.Z. Kiss, D. Muller, M.J. Licker, D. Morel, Adverse effects of methylene blue on the central nervous system. *Anesthesiology* **108**, 684–692 (2008)
- Y. Liu, L. Zong, C. Zhang, W. Liu, A. Fakhri, V.K. Gupta, Design and structural of Sm-doped SbFeO₃ nanopowders and immobilized on poly (ethylene oxide) for efficient photocatalysis and hydrogen generation under visible light irradiation. *Surface and interfaces* **26**, 101292 (2021)
- T. Wang, H. Wu, S. Zhao, W. Zhang, M. Tahir, Z. Wang, J. Wang, Interfacial polymerized and pore-variable covalent organic framework composite membrane for dye separation. *Chem. Eng. J.* **384**, 123347 (2020)
- W. Hu, L. Xie, H. Zeng, Novel sodium alginate-assisted MXene nanosheets for ultrahigh rejection of multiple cations and dyes. *J. Colloid Interface Sci.* **568**, 36–45 (2020)
- R. Tosik, S. Wiktorowski, Color removal and improvement of biodegradability of wastewater from dyes production using ozone and hydrogen peroxide. *Ozone Sci. Eng.* **23**, 295–302 (2001)
- X. Li, Q. Mei, L. Chen, H. Zhang, B. Dong, X. Dai, C. He, J. Zhou, Enhancement in adsorption potential of microplastics in sewage sludge for metal pollutants after the wastewater treatment process. *Water Res.* **157**, 228–237 (2019)
- J. Fu, J. Zhu, Z. Wang, Y. Wang, S. Wang, R. Yan, Q. Xu, Highly-efficient and selective adsorption of anionic dyes onto hollow polymer microcapsules having a high surface-density of amino groups: Isotherms, kinetics, thermodynamics and mechanism. *J. Colloid Interface Sci.* **542**, 123–135 (2019)
- R.V. Prihod'ko, N.M. Soboleva, Photocatalysis: Oxidative processes in water treatment. *J. Chem.* (2013). <https://doi.org/10.1155/2013/168701>
- N. Hao, Y. Nie, Z. Xu, C. Jin, T.J. Fyda, J.X. Zhang, Microfluidics-enabled acceleration of Fenton oxidation for degradation

- of organic dyes with rod-like zero-valent iron nanoassemblies. *J. Colloid Interface Sci.* **559**, 254–262 (2020)
12. M.L. Baynosa, A.H. Mady, D.R. Kumar, M.S. Sayed, D. Tuma, J.-J. Shim, Eco-friendly synthesis of recyclable mesoporous zinc ferrite@ reduced graphene oxide nanocomposite for efficient photocatalytic dye degradation under solar radiation. *J. Colloid Interface Sci.* **561**, 459–469 (2020)
 13. W. Liu, Y. Li, F. Liu, W. Jiang, D. Zhang, J.J. Liang, Visible-light-driven photocatalytic degradation of diclofenac by carbon quantum dots modified porous g-C₃N₄: Mechanisms, degradation pathway and DFT calculation. *Water Res.* **151**, 8–19 (2019)
 14. A. Akhondi, U. Feleni, B. Bethi, A.O. Idris, A. Hojjati-Najafabadi, Advances in metal-based vanadate compound photocatalysts: synthesis, properties and applications. *Synthesis and Sintering* **1**, 151–168 (2021)
 15. S. Venkatesh, K. Venkatesh, A.R. Quaff, Dye decomposition by combined ozonation and anaerobic treatment: Cost effective technology. *Journal of Applied Research and Technology* **15**, 340–345 (2017)
 16. L.W.J.J.o.h.m. Perelo, In situ and bioremediation of organic pollutants in aquatic sediments, 177 (2010) 81–89.
 17. P. Wang, J. Wang, X. Wang, H. Yu, J. Yu, M. Lei, Y. Wang, One-step synthesis of easy-recycling TiO₂-rGO nanocomposite photocatalysts with enhanced photocatalytic activity. *Applied Catalysis B* **132**, 452–459 (2013)
 18. S. Thangavel, K. Krishnamoorthy, S.-J. Kim, G. Venugopal, Designing ZnS decorated reduced graphene-oxide nanohybrid via microwave route and their application in photocatalysis. *J. Alloy. Compd.* **683**, 456–462 (2016)
 19. M. Malekzadeh, K.L. Yeung, M. Halali, Q. Chang, Synthesis of nanostructured Ag@ SiO₂-Penicillin from high purity Ag NPs prepared by electromagnetic levitation melting process. *Mater. Sci. Eng.* **102**, 616–622 (2019)
 20. S. Thangavel, S. Thangavel, N. Raghavan, K. Krishnamoorthy, G. Venugopal, Visible-light driven photocatalytic degradation of methylene-violet by rGO/Fe₃O₄/ZnO ternary nanohybrid structures. *J. Alloy. Compd.* **665**, 107–112 (2016)
 21. Z. Sabouri, A. Akbari, H.A. Hosseini, A. Hashemzadeh, M. Darroudi, Bio-based synthesized NiO nanoparticles and evaluation of their cellular toxicity and wastewater treatment effects. *J. Mol. Struct.* **1191**, 101–109 (2019)
 22. M. Mansoorianfar, H. Nabipour, F. Pahlevani, Y. Zhao, Z. Hussain, A. Hojjati-Najafabadi, H.Y. Hoang, R. Pei, Recent progress on adsorption of cadmium ion from water systems using metal-organic frameworks (MOFs) as an efficient class of porous materials. *Environ. Res.* **214**, 114113 (2022)
 23. L. Rao, Y. Zhu, Z. Duan, T. Xue, X. Duan, Y. Wen, A.S. Kumar, W. Zhang, J. Xu, A. Hojjati-Najafabadi, Lotus seedpods biochar decorated molybdenum disulfide for portable, flexible, outdoor and inexpensive sensing of hyperin. *Chemosphere* **301**, 134595 (2022)
 24. E. Baladi, F. Davar, A. Hojjati-Najafabadi, Synthesis and characterization of g-C₃N₄-CoFe₂O₄-ZnO magnetic nanocomposites for enhancing photocatalytic activity with visible light for degradation of penicillin G antibiotic. *Environ. Res.* **215**, 114270 (2022)
 25. A. Hojjati-Najafabadi, M. Mansoorianfar, T. Liang, K. Shahin, Y. Wen, A. Bahrami, C. Karaman, N. Zare, H. Karimi-Maleh, Y. Vasseghian, Magnetic-MXene-based nanocomposites for water and wastewater treatment: A review. *Journal of Water Process Engineering* **47**, 102696 (2022)
 26. A.I. Ayesh, A.A. Alyafei, R.S. Anjum, R.M. Mohamed, M.B. Abuharb, B. Salah, M. El-Muraikhi, Production of sensitive gas sensors using CuO/SnO₂ nanoparticles. *Appl. Phys. A* **125**, 1–8 (2019)
 27. M. Azmina, R.M. Nor, H. Rafeie, N. Razak, S. Sani, Z. Osman, Enhanced photocatalytic activity of ZnO nanoparticles grown on porous silica microparticles. *Appl. Nanosci.* **7**, 885–892 (2017)
 28. A. Shawky, S. El-Sheikh, A. Gaber, S.I. El-Hout, I.M. El-Sherbiny, A.I. Ahmed, Urchin-like CuS nanostructures: simple synthesis and structural optimization with enhanced photocatalytic activity under direct sunlight. *Appl. Nanosci.* **10**, 2153–2164 (2020)
 29. M. Abboud, M.A. Haija, R. Bel-Hadj-Tahar, A.T. Mubarak, I. Ismail, M.S. Hamdy, Highly ordered mesoporous flower-like NiO nanoparticles: synthesis, characterization and photocatalytic performance. *New J. Chem.* **44**, 3402–3411 (2020)
 30. H. Chen, A. Guo, Q. Ding, J. Zhu, L. Cheng, Dispersedly embedded loading of SnO₂ nanoparticles onto graphene nanosheets for highly efficient removal of organic dyes. *J. Nanophotonics* **11**, 026009 (2017)
 31. H.R. Rajabi, O. Khani, M. Shamsipur, V. Vatanpour, High-performance pure and Fe³⁺-ion doped ZnS quantum dots as green nanophotocatalysts for the removal of malachite green under UV-light irradiation. *J. Hazard. Mater.* **250**, 370–378 (2013)
 32. A.M. Taddesse, M. Alemu, T. Kebede, Enhanced photocatalytic activity of pnn heterojunctions ternary composite Cu₂O/ZnO/Ag₃PO₄ under visible light irradiation. *J. Environ. Chem. Eng.* **8**, 104356 (2020)
 33. S. Behjati, S. Sheibani, J. Herritsch, J.M. Gottfried, Photodegradation of dyes in batch and continuous reactors by Cu₂O-CuO nanophotocatalyst on Cu foils prepared by chemical-thermal oxidation. *Mater. Res. Bull.* **130**, 110920 (2020)
 34. A. Shawky, S.M. El-Sheikh, M.N. Rashed, S.M. Abdo, T.I. El-Dosoqy, Exfoliated kaolinite nanolayers as an alternative photocatalyst with superb activity. *J. Environ. Chem. Eng.* **7**, 103174 (2019)
 35. T. Munawar, F. Iqbal, S. Yasmeen, K. Mahmood, A. Hussain, Multi metal oxide NiO-CdO-ZnO nanocomposite—synthesis, structural, optical, electrical properties and enhanced sunlight driven photocatalytic activity. *Ceram. Int.* **46**, 2421–2437 (2020)
 36. T. Munawar, S. Yasmeen, M. Hasan, K. Mahmood, A. Hussain, A. Ali, M. Arshad, F. Iqbal, Novel tri-phase heterostructured ZnO–Yb₂O₃–Pr₂O₃ nanocomposite: structural, optical, photocatalytic and antibacterial studies. *Ceram. Int.* **46**, 11101–11114 (2020)
 37. M.N. Zafar, Q. Dar, F. Nawaz, M.N. Zafar, M. Iqbal, M.F. Nazar, Effective adsorptive removal of azo dyes over spherical ZnO nanoparticles. *J. Market. Res.* **8**, 713–725 (2019)
 38. K. Phiwang, S. Suphankij, W. Mekprasart, W. Pecharapa, Synthesis of CuO nanoparticles by precipitation method using different precursors. *Energy procedia* **34**, 740–745 (2013)
 39. P. Kar, S. Farsinezhad, X. Zhang, K. Shankar, Anodic Cu₂S and CuS nanorod and nanowall arrays: preparation, properties and application in CO₂ photoreduction. *Nanoscale* **6**, 14305–14318 (2014)
 40. D. Sobia, S. Mohammad, I. Azhar, Synthesis of zinc sulphide nanostructures by co-precipitation: Effect of doping on electro-optical properties. *Kenkyu Journal of Nanotechnology Nanoscience* **1**, 34–39 (2015)
 41. L.-N. Liu, J.-G. Dai, T.-J. Zhao, S.-Y. Guo, D.-S. Hou, P. Zhang, J. Shang, S. Wang, S. Han, A novel Zn (ii) dithiocarbamate/ZnS nanocomposite for highly efficient Cr⁶⁺ removal from aqueous solutions. *RSC Adv.* **7**, 35075–35085 (2017)
 42. M.S. Lucas, P.B. Tavares, J.A. Peres, J.L. Faria, M. Rocha, C. Pereira, C. Freire, Photocatalytic degradation of Reactive Black 5 with TiO₂-coated magnetic nanoparticles. *Catal. Today* **209**, 116–121 (2013)
 43. J. Kennedy, P. Murmu, J. Leveueur, A. Markwitz, J. Futter, Controlling preferred orientation and electrical conductivity of zinc oxide thin films by post growth annealing treatment. *Appl. Surf. Sci.* **367**, 52–58 (2016)

44. S. Marouf, A. Beniaiche, H. Guessas, A.J. Azizi, Morphological, structural and optical properties of ZnO thin films deposited by dip coating method. *Mater. Res.* **20**, 88–95 (2016)
45. D.C.T. Nguyen, L. Zhu, Q. Zhang, K.Y. Cho, W.-C. Oh, A new synergetic mesoporous silica combined to CdSe-graphene nanocomposite for dye degradation and hydrogen evolution in visible light. *Mater. Res. Bull.* **107**, 14–27 (2018)
46. X. Liu, C. Ma, Y. Yan, G. Yao, Y. Tang, P. Huo, W. Shi, Y. Yan, Hydrothermal synthesis of CdSe quantum dots and their photocatalytic activity on degradation of cefalexin. *Ind. Eng. Chem. Res.* **52**, 15015–15023 (2013)
47. T. Munawar, S. Yasmeen, F. Hussain, K. Mahmood, A. Hussain, M. Asghar, F. Iqbal, Physics, Synthesis of novel heterostructured ZnO-CdO-CuO nanocomposite: characterization and enhanced sunlight driven photocatalytic activity. *Mater. Chem. Phys.* **249**, 122983 (2020)
48. T. Munawar, F. Mukhtar, M.S. Nadeem, K. Mahmood, M. Hasan, A. Hussain, A. Ali, M. Arshad, F. Iqbal, Physics, Novel direct dual-Z-scheme ZnO-Er₂O₃-Nd₂O₃@ reduced graphene oxide heterostructured nanocomposite: synthesis, characterization and superior antibacterial and photocatalytic activity. *Mater. Chem. Phys.* **253**, 123249 (2020)
49. T. Munawar, M.S. Nadeem, F. Mukhtar, A. Azhar, M. Hasan, K. Mahmood, A. Hussain, A. Ali, M. Arshad, M.A. Nabi, Synthesis, characterization, and antibacterial study of novel Mg_{0.9}Cr_{0.05}M_{0.05}O (M= Co, Ag, Ni) nanocrystals. *Phys. B* **602**, 412555 (2021)
50. T. Munawar, M.S. Nadeem, F. Mukhtar, M. Riaz, F. Iqbal, Sol-gel synthesis of Cu_{0.9}Zn_{0.05}M_{0.05}O (M= Cr Co, Cd) nanocrystals for removal of pollutant dyes and bacterial inactivation. *J. Mater. Sci.* **32**, 14437–14455 (2021)
51. T. Munawar, M.N. Rehman, M.S. Nadeem, F. Mukhtar, S. Manzoor, M.N. Ashiq, F. Iqbal, Compounds, Facile synthesis of Cr-Co co-doped CdO nanowires for photocatalytic, antimicrobial, and supercapacitor applications. *J. Alloy. Compd.* **885**, 160885 (2021)
52. T. Munawar, F. Mukhtar, M.S. Nadeem, S. Manzoor, M.N. Ashiq, K. Mahmood, S. Batool, M. Hasan, F. Iqbal, Compounds, Fabrication of dual Z-scheme TiO₂-WO₃-CeO₂ heterostructured nanocomposite with enhanced photocatalysis, antibacterial, and electrochemical performance. *J. Alloy. Compd.* **898**, 162779 (2022)
53. T. Munawar, F. Mukhtar, M.S. Nadeem, K. Mahmood, A. Hussain, A. Ali, M. Arshad, M.A. un Nabi, F.J. Iqbal, Structural, optical, electrical, and morphological studies of rGO anchored direct dual-Z-scheme ZnO-Sm₂O₃-Y₂O₃ heterostructured nanocomposite: an efficient photocatalyst under sunlight. *Solid State Sci.* **106**, 106307 (2020)
54. A. Serrà et al., Highly active ZnO-based biomimetic fern-like microleaves for photocatalytic water decontamination using sunlight. *Appl. Catal.B* **248**, 129–146 (2019)
55. Y.I. Choi et al., Fabrication of ZnO, ZnS, Ag-ZnS, and Au-ZnS microspheres for photocatalytic activities, CO oxidation and 2-hydroxyterephthalic acid synthesis. *J. Alloys Compounds* **675**, 46–56 (2016)
56. X.-S. Hu et al., Preparation of flower-like CuS by solvothermal method and its photodegradation and UV protection. *J. Alloys Compounds* **674**, 289–294 (2016)
57. B. Ahmed et al., Shape induced (spherical, sheets and rods) optical and magnetic properties of CdS nanostructures with enhanced photocatalytic activity for photodegradation of methylene blue dye under ultra-violet irradiation. *J. Alloys Compounds* **679**, 324–334 (2016)
58. D. Pathania et al., Photocatalytic degradation of highly toxic dyes using chitosan-g-poly (acrylamide)/ZnS in presence of solar irradiation. *J. Photochem. Photobiol. A* **329**, 61–68 (2016)
59. S.A.B. Asif, S.B. Khan, Visible light functioning photocatalyst based on Al₂O₃ doped Mn₃O₄ nanomaterial for the degradation of organic toxin. *Nanoscale Res. Lett.* **10**(1), 1–10 (2015)
60. G. Poongodi, R.M. Kumar, R.J.C.I. Jayavel, Influence of S doping on structural, optical and visible light photocatalytic activity of ZnO thin films. *Ceram. Int.* **40**(9), 14733–14740 (2014)
61. S. Ramezanpour, I. Sheikhsheoie, Synthesis, characterization and photocatalytic properties of V-doped Mn₃O₄ nanoparticles as a visible light-activated photocatalyst. *J. Molecular Liquids* **231**, 64–71 (2017)
62. A. Sukhdev et al., Synthesis, phase transformation, and morphology of hausmannite Mn₃O₄ nanoparticles: photocatalytic and antibacterial investigations. *Heliyon* **6**(1), e03245 (2020)
63. A. Jamal et al., Hydrothermally preparation and characterization of un-doped manganese oxide nanostructures: Efficient photocatalysis and chemical sensing applications. *Micro Nanosyst.* **5**(1), 22–28 (2013)

Publisher's Note Springer Nature remains neutral with regard to jurisdictional claims in published maps and institutional affiliations.

Springer Nature or its licensor (e.g. a society or other partner) holds exclusive rights to this article under a publishing agreement with the author(s) or other rightsholder(s); author self-archiving of the accepted manuscript version of this article is solely governed by the terms of such publishing agreement and applicable law.